### Title

Polariton-based band gap and generation of surface acoustic waves in acoustic superlattice lithium niobate




### Journal

Journal of Applied Physics, 114(5)

### ISSN

0021-8979



### Authors

Yudistira, Didit
Boes, Andreas
Janner, Davide
et al.



### Publication Date

2013-08-07

### DOI

10.1063/1.4817271

Peer reviewed

AIP | Journal of Applied Physics

# Polariton-based band gap and generation of surface acoustic waves in acoustic superlattice lithium niobate

Didit Yudistira, Andreas Boes, Davide Janner, Valerio Pruneri, James Friend, and Arnan Mitchell

Citation: Journal of Applied Physics **114**, 054904 (2013); doi: 10.1063/1.4817271
View online: http://dx.doi.org/10.1063/1.4817271
View Table of Contents: http://scitation.aip.org/content/aip/journal/jap/114/5?ver=pdfcov
Published by the AIP Publishing

# Polariton-based band gap and generation of surface acoustic waves in acoustic superlattice lithium niobate

Didit Yudistira,[1] Andreas Boes,[1,2] Davide Janner,[3] Valerio Pruneri,[3,4] James Friend,[5] and Arnan Mitchell[1,2]
[1]*School of Electrical and Computer Engineering, RMIT University, VIC 3001, Melbourne, Australia*
[2]*ARC Centre of Excellence for Ultrahigh bandwidth Devices and Optical Systems, RMIT University, VIC 3001, Melbourne, Australia*
[3]*ICFO-Institut de Ciencies Fotoniques, Mediterranean Technology Park, 08860 Castelldefels (Barcelona), Spain*
[4]*ICREA-Institució Catalana de Recerca i Estudis Avançats, E-08010 Barcelona, Spain*
[5]*Micro Nano physics Research Laboratory, RMIT University, VIC 3001, Melbourne and the Melbourne Centre for Nanofabrication, VIC 3166, Clayton, Australia*

(Received 2 June 2013; accepted 16 July 2013; published online 5 August 2013)

We report the presence of surface acoustic wave (SAW) band gap on acoustic superlattice (ASL) in a single-crystal lithium niobate structure. The band gap behavior is determined by calculating the SAW band structure and also by simulating the transmission of an acoustic wave through a finite length section of ASL using finite element analysis. The calculated band gap appears at a frequency twice the value expected from purely acoustic Bragg scattering. We have identified the band gap as originating from a polariton-based mechanism due to the coupling between the electromagnetic wave and the surface vibrations. We have examined the influence of the band gap on SAW generation with the ASL and have shown that the calculated frequency resonance of the SAW lies in the vicinity of the upper stop-band edges. This results in the localization of the SAW in the ASL. Experimental confirmation is achieved through direct measurement of the SAW displacement by laser vibrometry on an actual ASL SAW transducer. The localization of generated SAW to the ASL transducer is observed confirming the prediction of the existence of a band gap. © *2013 AIP Publishing LLC*. [http://dx.doi.org/10.1063/1.4817271]

## I. INTRODUCTION

Band structures are well-known phenomena in solid-state physics. In real atomic crystals, a band structure is formed by a periodic potential of the electrons that can allow (band pass) or forbid (band gap) the electrons to propagate. Analogously, in artificial crystals such as composite materials, the periodic modulation of the corresponding physical parameters (refractive index, acoustic impedance, etc.) can cause waves to experience Bragg scattering, leading to the formation of band structures governed by similar physics. As a prominent example, it is well known that so called photonic crystal structures with strong periodic spatial modulation of refractive index can exhibit photonic band gaps, preventing the propagation of optical waves with certain wave vectors.[1] This fact has been employed for the manipulation of light, the construction of novel laser geometries, and suppression of spontaneous emission.[2] In a similar manner, *phononic* crystals, structure with periodic *elastic* properties, can exhibit a so-called *phononic* band gap[3,4] preventing the propagation of acoustic waves with certain wave vectors. Phononic band gap structures have been used to form perfect acoustic mirrors, acoustic metamaterials,[5] and achieve acoustic confinement.[6] In fact, Bragg scattering is not the only mechanism to form a band structure or band gap. A strong coupling between electromagnetic (EM) and material polarization waves has been shown as another mechanism for creating a band gap structure.[7] Such coupling mechanism, in the quantum of the coupled mode, is called a *polariton*.[7] In a piezoelectric superlattice structure, where the piezoelectric coefficient is spatially modulated, a phonon-polariton quasiparticle can be established as a consequence of the coupling between the EM wave and the superlattice vibration (phonon).[8–12] Furthermore, coupling between EM waves and both transverse superlattice vibrations (transverse phonons) and, individually, longitudinal ones (longitudinal phonons) have been demonstrated to exist because of the anisotropic nature of all piezoelectric materials.[10]

Recently, a piezoelectric superlattice configured as a semi-infinite or surface-terminated lithium niobate ($LiNbO_3$) substrate—*acoustic superlattice* (ASL)— has been used to realize a new kind of surface acoustic waves (SAW) transducer.[13,14] This structure offers an alternative to SAW generation compared to interdigital transducers (IDTs);[15] the method has been demonstrated experimentally.[13,14,16] Characterization of the transducer by means of radio frequency (RF) and acousto-optical measurements has enabled direct observation of the excited SAW displacement.[14,16] The use of such a transducer in an integrated SAW-based, acousto-optic filter has recently been reported.[16,17]

The fact that the SAW can be excited on the ASL is directly related to the coupling between the EM wave excited by the electrodes on the ASL surface and the superlattice SAW vibration (surface phonons). In accordance to the aforementioned works,[8–12] this would also then result in

 

the formation of phonon-polariton, which differs from the results presented in Ref. 10, where the phonon-polaritons originate from the coupling between EM waves and bulk transverse and longitudinal lattice vibrations. The presence of phonon-polaritons can lead to the formation of a band gap;[7] hence, we hypothesize that a polariton-like based SAW band gap would be formed in the ASL. This band gap would influence the characteristics of the SAW generated by an ASL based transducer potentially causing the generated SAW to be localized, trapped within the band gap. This behavior is significantly different from the propagating SAW typical of standard IDTs.

We test our hypothesis in this work with finite element analysis simulations to calculate the band structures of the ASL. The ASL structure being considered is derived from periodic domain inversion of *Z*-cut $LiNbO_3$ substrate achieved using electric field poling.[18] The domain walls were taken to be parallel to the *ZY* plane and distributed periodically along the *x*-axis of SAW propagation, we applied a mode-sorting technique to obtain the SAW bands pass representing the band structure, allowing us to filter out spurious modes generated by the calculation due to the finite thickness of the model structure being considered in the simulation. Transmission analysis on a finite periodic structure was carried out to confirm the existence of the SAW band gap in physically achievable design. Furthermore, we numerically and experimentally studied the presence of the band gap on the SAW generation in the ASL-based SAW transducer, including the localization of the SAW to the finite ASL transducer. Laser interferometric vibrometry was used in experiments to quantify the generation and localization of the SAW inside the ASL. Here, we focus our attention solely on the search for the SAW band gap. An accompanying polariton-induced band gap may exist in electromagnetic branch; this aspect is an interesting topic for distinct investigation.

The paper is organized as follows. In Sec. II, we present the model and methods for calculating the SAW band structure that includes SAW transmission, SAW generation on the ASL structure, and the experimental procedure to measure the profile of the excited SAW. In Sec. III, we present and discuss the results from the finite element analysis and experimental results. Section IV presents the conclusions.

## II. MODEL AND METHODS

Figure 1 illustrates the numerical model of the structure considered in this study. In the numerical modeling, the lateral width of the structure is assumed to be much larger than the lattice period ($a$), and so there is no variation of the fields along the *y*-axis $\partial/\partial y = 0$; the structure is semi-infinite in the thickness with termination at the surface. The electromechanically coupled equation set consisting of the piezoelectric coupling equations, and the Maxwell and elasticity equations governing the propagation of EM and acoustic waves, respectively, to be solved via the finite element method, are given by[19]

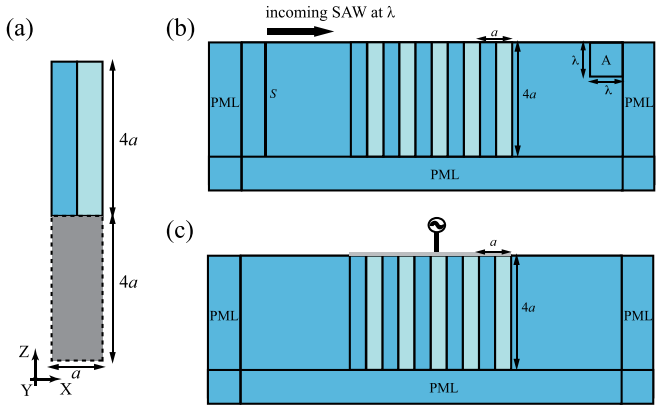


FIG. 1. (a) 2D representation of the unit cell used for band structure calculations, where the blue and the grey areas denote the $LiNbO_3$ layer and the artificial layer, respectively. A Floquet-Bloch boundary condition is imposed in the *x* direction. (b) Model structure used for transmission computations. Stress free boundary condition is applied on the surface structure and the remaining boundaries were terminated by the PMLs to prevent reflection from the domain boundaries. The field source is inserted over line *S* and the transmission is calculated over the area A. (c) Model structure is used for SAW generation computation, which is similar to (b) except on the surface embracing the ASL, Dirichlet boundary condition was imposed by applying RF potential $V_{RF} = 1$ V, and the SAW incidence to the ASL was disregarded. In all figures, positive and negative domains are indicated by dark and light blue areas, respectively.

$$\begin{cases} \mathbf{T} = C^E : (\nabla_S \cdot \mathbf{u}) - \mathbf{e}^T(x) \cdot \mathbf{E}; & \text{(a)} \\ \mathbf{D} = \varepsilon^S \cdot \mathbf{E} + \mathbf{e}(x) : (\nabla_S \cdot \mathbf{u}); & \text{(b)} \\ \nabla^2 \mathbf{E} = \mu_0 \partial_t^2 \mathbf{D}; & \text{(c)} \\ \nabla \cdot \mathbf{T} = \rho \partial_t^2 \mathbf{u}. & \text{(d)} \end{cases} \quad (1)$$

Here, **T**, **u**, **E**, and **D** are stress, elastic field, electric field, and electrical displacement, respectively. $\mathbf{C}^E$, $\rho$, and $\boldsymbol{\varepsilon}^S$ are stiffness, density, and dielectric constants. The periodically modulated piezoelectric coefficients are defined as $\mathbf{e}(x) \equiv f(x)\mathbf{e}$, where $f(x)$ is $+1$ in positive domains and $-1$ in negative domains, respectively. For simplicity, the thickness of the positive and the negative domains were set to $a/2$, where $a$ is the lattice period.

The SAW band structures were calculated on an infinite periodic system by considering its corresponding unit cell as shown in Fig. 1(a). Floquet-Bloch conditions were imposed by applying a periodic boundary condition along the *x* axis. A stress-free boundary condition was imposed on the surface of the structure; the normal component of the electric displacement is zero. In the finite element model, as the SAW decays exponentially roughly one-wavelength from the surface, it was reasonable to set the thickness of the layer accounting for the $LiNbO_3$ substrate to be four times the lattice constant, or $4a$, where here we assume that the exciting SAW wavelength is equal to the lattice constant of the ASL.[13] Furthermore, to avoid the excitation of spurious modes, particularly the SAW that may propagate at the free bottom surface of the $LiNbO_3$ layer, an additional $4a$-thick artificial layer with high acoustic velocity compared with $LiNbO_3$ was introduced, as shown in Fig. 1(a). In the simulation, all the modes satisfying Eq. (1) and the boundary conditions, including the bulk modes, were also found due to the

finite system. Therefore, in order to distinguish the surface modes from the bulk modes, a mode-sorting technique based on the depth-weighted strain energy Density Of Energy (DOE) was implemented

$$DOE = z_{\max} - \frac{\iint_D z(S_z S_z^* + S_x S_x^*)dxdz}{\iint_D (S_z S_z^* + S_x S_x^*)dxdz}. \quad (2)$$

$S_x$ and $S_y$ denote the $x$- and $y$- directed strains.

For the transmission calculations, the model shown in Fig. 1(b) was considered. An incoming SAW with a spectrum $\lambda$ was modeled by inserting the SAW field solution of an infinite IDT structure into the model via line $S$ as indicated in Fig. 1(b). A stress free boundary condition was employed at the surface and the remaining boundaries were terminated by the perfectly matched layers (PMLs). The SAW transmittance was calculated over region A (see Fig. 1(b)), based upon the ratio of mechanical energy of the transmitted waves in the structure with a periodic modulation, to the mechanical energy present without the periodic modulation.

The model in Fig. 1(c) was used to determine the generation of the SAW in the periodic structure. The structure is somewhat similar to the case of the transmission calculation, but here a Dirichlet boundary condition was imposed on the surface boundary enclosing the lattice by applying RF potential $V_{RF} = 1$ V and there was no SAW incidence to the ASL. In order to characterize of the generated SAW from the ASL, the conductance $G$ with respect to excitation frequency was calculated to determine the characteristics of the SAW-generating ASL.

As direct experimental evidence, the localized SAW generated by the ASL-based transducer was observed using laser vibrometry. The setup used is similar to the one described in Ref. 20. The crystal used was a $Z$-cut 500-$\mu$m-thick single crystal $LiNbO_3$. Electric field poling at a room temperature[18] was used to form the ASL, with a period of $a = 20\,\mu$m; the ASL consisted of 500 periods. A co-planar aluminum electrode with thickness of 200 nm and the width and gap of 60 $\mu$m was deposited on the $z$ face of the sample and aligned along $x$-axis. The reflection coefficient ($S_{11}$) of the ASL was measured (Agilent PNX Series Network Analyzer) to determine the resonance frequency of the SAW. Once the SAW resonance was determined, laser vibrometry measurements were performed by scanning the ASL along the $x$-axis with the laser probe.

## III. RESULTS AND DISCUSSION

In determining the band structure, the simulation was performed over a one-dimensional Brillouin zone that extends from $k_x = 0$ to $k_x = \pi/a$. The results of the simulation are shown in the *reduced-zone scheme* with the SAW frequency modes normalized using the lowest bulk velocity $c$. For comparison the SAW band structure for a homogeneous unit cell was also calculated. This also enabled validation of the mode sorting mechanism used in the simulation. The results are

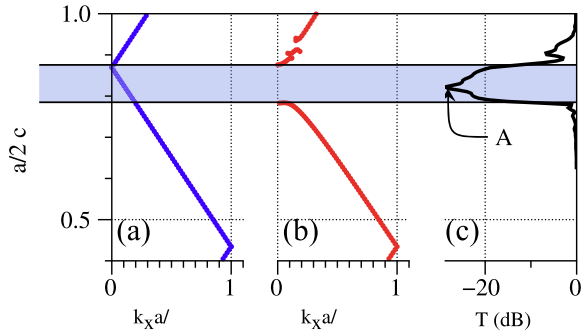


FIG. 2. Computed band structures of (a) homogeneous or single crystal Z-cut $LiNbO_3$, (b) ASL with lattice period $a$. (c) Calculated transmission spectrum from the SAW propagating through ASL structure. Shaded blue area represents the obtained SAW band gap.

presented in Figs. 2(a) and 2(b) for the homogeneous and the ASL structures, respectively. Figure 2(a) shows that the medium is non-dispersive as expected. The calculated slope is equal to the SAW velocity ($v_{SAW}$), confirming the SAW band structure. With the introduction of piezoelectric reversal (i.e., $\mathbf{e}(x) \equiv \mathbf{e}f(x)$), we can clearly observe in Fig. 2(b) the existence of a frequency gap at the center of the Brillouin zone on the vertical axis indicated by the blue region for which there is no associated wave vector $k_x$. The band gap is also confirmed from the transmission spectra presented in Fig. 2(c), as calculated from the finite ASL structure depicted in Fig. 1(b) with 12 periods that are sandwiched between the incident and transmission regions, respectively. Here, the gap is indicated by the dip in the transmission curve implying a strong SAW reflection and strong exponential decay in the lattice clearly shown in Fig 3 for a SAW propagating into the ASL with a frequency chosen from Fig. 2(c) at point A, which lies within the band gap of the ASL structure. In order to understand the propagation of the SAW within the ASL, the top panel of Fig. 3 displays the calculated total displacement of the SAW. A narrow band gap situated slightly above the SAW band gap shown in Fig 2(b) could correspond to a pseudo or leaky SAW band gap.[21] This is also confirmed by the transmission curve in Fig. 2(c), which exhibits a subtle dip at a higher frequency.

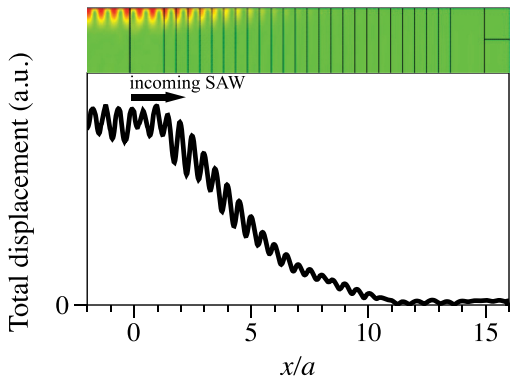


FIG. 3. Calculated total SAW displacement for a frequency indicated by point A in Fig. 2(c) suggests that the incident SAW is almost totally reflected and shows a strong exponential decay in the lattice. The top panel displays the SAW profile as propagating through ASL structure.

To begin discussion of the above results, we would like to note that the SAW band gap has been known to exist on single $LiNbO_3$ crystal with periodic metal strips deposited upon it.[15] Although there is some similarities to the structure that we present here, the formation of the SAW band gap in the structure relies on the Bragg scattering mechanism, a result of a periodic change in the acoustic impedance $Z = \rho v_{SAW}$ due to the concomitant charge in the electrical boundary conditions from metal strip to gap and the mass loading placed upon the substrate by the metal strips. Furthermore, the lowest, purely acoustic Bragg gap appears at a frequency given by $\omega_B = v_{SAW}\pi/a$. In the present work, the acoustic impedance of both positive and negative domains in the ASL structure is equal,[10] implying that the mechanism of band gap formation must be different. Furthermore, as shown in Fig. 2(b) the band gap appears at a higher frequency, twice $(2\omega_B)$ what would be expected from the Bragg gap. This implies that the formation of the SAW band gap in the ASL is clearly not due to a purely acoustic Bragg condition. The formation of the gap is instead due to the polariton-based mechanism caused by the coupling between the EM waves and the surface lattice vibrations on the ASL. This can be explained using the model of Eq. (1) as follows. In the infinite periodic structure, the surface phonons that propagate as Bloch waves are coupled to the EM waves through a piezoelectric coupling given by Eq. (1b). The induced EM waves may then in turn excite counter-propagating surface phonons through Eq. (1a) that will then interfere with the original ones. The superposition of the two surface phonons will thus result in the formation of the gap.

The fact that the gap appears at twice the frequency, $2\omega_B$, of the Bragg gap can be explained by performing Fourier analysis on the perturbation factor denoted by $P(x)$, which is given in the following equation of acoustic vibration derived from Eq. (1):

$$\nabla \cdot [C^E : (\nabla_S \cdot \mathbf{u})] + \rho\omega^2 \mathbf{u} = P(x)\mathbf{M} : (\nabla_S \cdot \mathbf{u}). \quad (3)$$

Derivation of Eq. (3) from Eq. (1) is given in the appendix where the matrix $\mathbf{M}$ is given by Eq. (A3). The perturbation factor $P(x)$ is given by $P(x) = f'(x)f(x) = \sum_{n=-\infty}^{\infty} \delta(x - na/2)$, a periodic delta distribution with a period of $a/2$. The corresponding Fourier transform of $P(x)$ is given by $\Im[\sum_{n=-\infty}^{\infty} \delta(x - na/2)] = 4\pi/a \sum_{n=-\infty}^{\infty} \delta(k - n4\pi/a)$ that has discrete values at $k_n = \pm 4\pi/a, \pm 8\pi/a, \ldots$, or $k_x = \pm 2\pi/a, \pm 4\pi/a, \ldots$, corresponding to $\omega = 2\omega_B, 4\omega_B, \ldots$.

The generation of the SAW by the ASL-based transducer was next computed using the structure depicted in Fig. 1(c). In the simulation, the input frequency $f(k_x) = v_{SAW}k_x/2\pi$ was varied around the frequency gap obtained from the results of Fig. 1(b). For each frequency, the conductance $(G)$ was determined and the result is presented in Fig. 4. A pronounced peak of conductance is evident at a particular frequency (labeled A′ in Fig. 4.), indicating a strong mechanical energy generated by the transducer. From this peak, the resonance frequency of $f_R \approx v_{SAW}a$ is determined, confirming the generation of SAW. By comparing the location of the peak against the position of the band gap illustrated as the shaded blue area, the calculated resonance frequency of the SAW lying in the vicinity of the upper edges of the band gap is obtained. This result implies that the excited SAW is a non-propagating standing wave, trapped in the cavity formed by the ASL confirmed further by the calculated SAW displacement profile at frequency $f_R$ shown in Fig. 5.

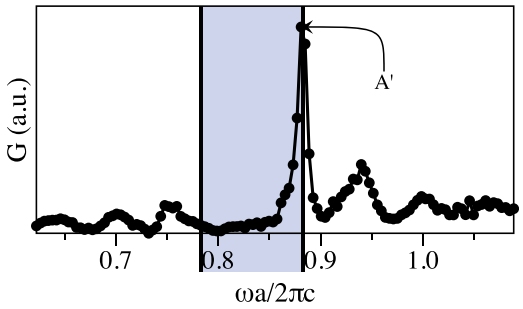


FIG. 4. Calculated conductance $G$ as a function of RF frequency on a finite ASL transducer with 12 lattice periods. The strong maxima at A′ suggest a strong mechanical energy generated by the transducer in the form of SAW, which lies in the vicinity of the upper stop band edges shown by the shaded blue area. The line is only a guide for the eye.

To experimentally demonstrate the localization of the SAW in the ASL transducer, the scattering parameter $S_{11}$ of the ASL transducer was first measured. The measurement result is shown in Fig. 6(a), where the dip in $S_{11}$ at the frequency of 190 MHz is observed indicating the SAW generation at the expected frequency.[17] To obtain the displacement profile of the excited SAW along the ASL, the electrodes were driven at the SAW resonance frequency of 190 MHz, and a laser vibrometry measurement was carried out to visualize the generated acoustic wave. The measured SAW displacement is shown in Fig. 6(b). It is evident that the amplitude of the vibration is mostly localized within the ASL, and the distance between amplitude maxima as shown in the inset of Fig. 6(b) is 20 $\mu$m, confirming the SAW generation. This measurement also confirms that the excited SAW by the ASL is in the form of a non-propagating standing wave and is localized within the ASL, consistent with the numerical predications. The measured displacement profile does not have the canonical sinusoidal shape predicted by the idealized theory. While the theory assumes field invariance in the $y$-direction, being essentially single mode, the

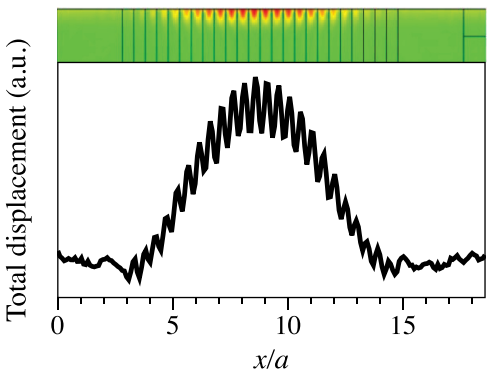


FIG. 5. The calculated SAW displacement profile at SAW resonance frequency, calculated at A′ in Fig. 4, confirms that the generated SAW is a standing wave and localized within the ASL.

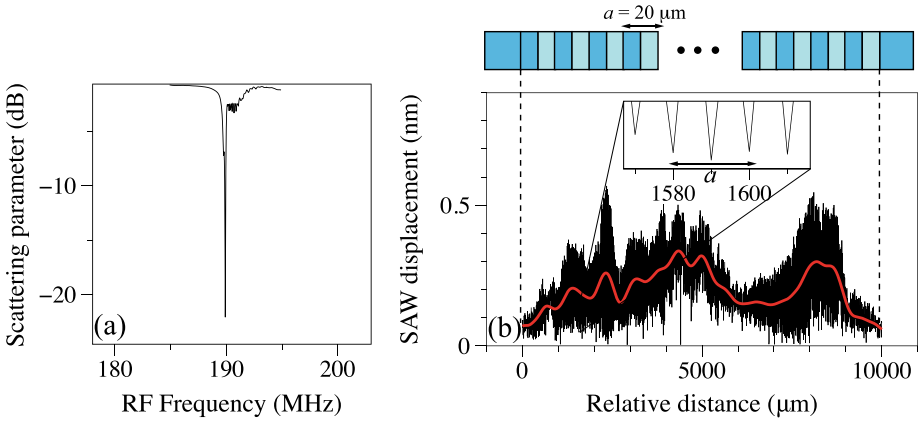


FIG. 6. (a) Measured $S_{11}$ from ASL transducer with 20 $\mu$m lattice period. Strong dip located around 190 MHz indicates the expected SAW generation on the ASL transducer. (b) The amplitude of SAW vibrations along the ASL length, as measured using laser vibrometry for a frequency of 190 MHz, confirms the localization of the generated SAW within the ASL. The red line represents the local mean value of the vibration.

measured sample actually has a displacement variation along the $y$-direction due to the use of the coplanar electrodes: multiple resonant paths exist for the acoustic resonance along both the $x$- and $y$-directions. A more canonical profile may be obtained if the ASL transducer were formed within a single mode acoustic waveguide.

## IV. CONCLUSIONS

In summary, we provided evidence that ASL structures can induce a SAW band gap. This band gap behavior was determined by calculating the SAW band structure and also by simulating the transmission of an acoustic wave through a finite length section of ASL using finite element analysis. We have shown that the calculated band gap appears at a frequency twice the value expected from purely acoustic Bragg scattering. We have identified the band gap as originating from a polariton-based mechanism due to the coupling between the EM wave and the surface vibrations. To examine the influence of the band gap on SAW generation with the ASL, we have calculated the SAW generation on a finite ASL. We have shown that the calculated frequency resonance of the SAW lies in the vicinity of the upper stop-band edges. This results in the localization of the SAW in the ASL. Experimental confirmation was achieved through direct measurement of the SAW displacement by laser vibrometry on an actual ASL SAW transducer. The localization of generated SAW to the ASL transducer was observed confirming the prediction of the existence of a band gap.

## ACKNOWLEDGMENTS

D.Y. would like to acknowledge Bahram Djafari Rouhani for fruitful discussion. This work was partly supported by Ministerio de Educación y Ciencia (Spain) through grant TEC2010-14832 and Ramon y Cajal program. J.F. acknowledges the Vice-Chancellors Senior Research Fellowship from RMIT University and the MCN SeniorTech fellowship from the Melbourne Centre for Nanofabrication. A.M. time commitment to this project was under the ARC Centre of Excellence program (CE110001018). However, this project was not supported with funding from this centre.

## APPENDIX

If we substitute Eq. (1a) and the piezoelectric modulation $\mathbf{e}(x) \equiv \mathbf{e}f(x)$ into Eq. (1d). So that, Eq. (1d) in matrix form now reads

$$\begin{pmatrix} C_{11}\partial_x^2+2C_{14}\partial_y\partial_z+C_{66}\partial_y\partial_x+C_{44}\partial_z^2 & C_{12}\partial_y\partial_x+(C_{14}+C_{44})\partial_x\partial_z+C_{66}\partial_y\partial_x & (C_{13}+C_{44})\partial_x\partial_z+2C_{14}\partial_y\partial_x \\ C_{66}\partial_x^2+2C_{14}\partial_x\partial_z+C_{12}\partial_y\partial_x & C_{66}\partial_x^2-2C_{14}\partial_y\partial_z+C_{11}\partial_y^2+C_{44}\partial_z^2 & C_{14}\partial_x^2-C_{14}\partial_y^2+(C_{13}+C_{44})\partial_y\partial_z \\ (C_{13}+C_{44})\partial_x\partial_z+2C_{14}\partial_y\partial_x & C_{44}\partial_x^2-C_{14}\partial_y^2+(C_{13}+C_{44})\partial_y\partial_z & C_{44}\partial_x^2+C_{44}\partial_y^2+C_{33}\partial_z^2 \end{pmatrix}$$

$$\times \begin{pmatrix} u_x \\ u_y \\ u_z \end{pmatrix} + \rho\omega^2 \begin{pmatrix} u_x \\ u_y \\ u_z \end{pmatrix} = f'(x) \begin{pmatrix} 1 & 0 & 0 & 0 & 0 & 0 \\ 0 & 0 & 0 & 0 & 0 & 1 \\ 0 & 0 & 0 & 0 & 1 & 0 \end{pmatrix} \begin{pmatrix} 0 & 0 & 0 & 0 & e_{15} & -e_{22} \\ -e_{22} & e_{22} & 0 & e_{15} & 0 & 0 \\ e_{31} & e_{31} & e_{33} & 0 & 0 & 0 \end{pmatrix}^T \begin{pmatrix} E_x \\ E_y \\ E_z \end{pmatrix}. \quad \text{(A1)}$$

Let us assume that the electric field solution $\mathbf{E}$ inside the crystal is proportional to $e^{i(\omega t-\chi z-k_x x)}$ where $\chi$ denotes the $z$-component of the wave number. From Eqs. (1b) and (1c), and inserting the field solution into Eq. (1c), the electric field is given by

$$\begin{pmatrix} E_x \\ E_y \\ E_z \end{pmatrix} = f(x) \begin{pmatrix} -k_x^2 + \mu_0\omega^2\varepsilon_{11} & 0 & 0 \\ 0 & \mu_0\omega^2\varepsilon_{22} & 0 \\ 0 & 0 & \chi^2 + \mu_0\omega^2\varepsilon_{11} \end{pmatrix}^{-1} \times \begin{pmatrix} 0 & 0 & 0 & 0 & e_{15} & -e_{22} \\ -e_{22} & e_{22} & 0 & e_{15} & 0 & 0 \\ e_{31} & e_{31} & e_{33} & 0 & 0 & 0 \end{pmatrix} \begin{pmatrix} \partial_x & 0 & 0 & 0 & \partial_z & \partial_y \\ 0 & \partial_y & 0 & \partial_z & 0 & \partial_x \\ 0 & 0 & \partial_z & \partial_y & \partial_x & 0 \end{pmatrix} \begin{pmatrix} u_x \\ u_y \\ u_z \end{pmatrix}. \quad \text{(A2)}$$

Inserting (A2) into (A1), we obtain a wave motion equation for acoustic phonon as given by Eq. (2), where matrix **M** is

$$\mathbf{M} \equiv \frac{1}{(-k_x^2 + \mu_0\omega^2\varepsilon_{11})(\mu_0\omega^2\varepsilon_{22})(\chi^2 + \mu_0\omega^2\varepsilon_{11})} \times \begin{pmatrix} M_{11} & M_{12} & M_{13} & M_{14} & 0 & 0 \\ 0 & 0 & 0 & 0 & M_{25} & M_{26} \\ 0 & 0 & 0 & 0 & M_{35} & M_{36} \end{pmatrix} \quad \text{(A3)}$$

where

$$M_{11} = e_{22}^2(-k_x^2 + \mu_0\omega^2\varepsilon_{11})(\chi^2 + \mu_0\omega^2\varepsilon_{11}) + e_{31}^2(-k_x^2 + \mu_0\omega^2\varepsilon_{11})(\mu_0\omega^2\varepsilon_{22}),$$

$$M_{12} = -e_{22}^2(-k_x^2 + \mu_0\omega^2\varepsilon_{11})(\chi^2 + \mu_0\omega^2\varepsilon_{11}) + e_{31}^2(-k_x^2 + \mu_0\omega^2\varepsilon_{11})(\mu_0\omega^2\varepsilon_{22})$$

$$M_{13} = e_{31}e_{33}(-k_x^2 + \mu_0\omega^2\varepsilon_{11})(\mu_0\omega^2\varepsilon_{22}),$$

$$M_{14} = -e_{15}e_{22}(-k_x^2 + \mu_0\omega^2\varepsilon_{11})(\chi^2 + \mu_0\omega^2\varepsilon_{11}),$$

$$M_{25} = -e_{22}e_{15}(\chi^2 + \mu_0\omega^2\varepsilon_{11})(\mu_0\omega^2\varepsilon_{22}),$$

$$M_{26} = e_{22}^2(\chi^2 + \mu_0\omega^2\varepsilon_{11})(\mu_0\omega^2\varepsilon_{22}),$$

$$M_{35} = e_{15}^2(\chi^2 + \mu_0\omega^2\varepsilon_{11})(\mu_0\omega^2\varepsilon_{22}),$$

$$M_{36} = -e_{15}e_{22}(\chi^2 + \mu_0\omega^2\varepsilon_{11})(\mu_0\omega^2\varepsilon_{22}).$$


[1]E. Yablonovitch, Phys. Rev. Lett. **58**, 2059 (1987).
[2]J. D. Joannopoulos, *Photonic Crystals: Modeling the Flow of Light*, 2nd ed. (Princenton Univ. Press, 2008).
[3]M. S. Kushwaha, P. Halevi, L. Dobrzynski, and B. Djafari-Rouhani, Phys. Rev. Lett. **71**, 2022 (1993).
[4]M. Sigalas and E. N. Economou, Solid State Commun. **86**, 141 (1993).
[5]N. Fang, D. Xi, J. Xu, M. Ambati, W. Srituravanich, C. Sun, and X. Zhang, Nature Mater. **5**, 452 (2006).
[6]J. Hwan Oh, I. Kyu Lee, P. Sik Ma, and Y. Young Kim, Appl. Phys. Lett. **99**, 083505 (2011).
[7]K. Huang, *Dynamical Theory of Crystal Lattices* (Oxford Univ. Press, Incorporated, 1954).
[8]Y. Zhu, X. Zhang, Y. Lu, Y. Chen, S. Zhu, and N. Ming, Phys. Rev. Lett. **90**, 053903 (2003).
[9]C. Huang and Y. Zhu, Phys. Rev. Lett. **94**, 117401 (2005).
[10]X. Zhang, R. Zhu, J. Zhao, Y. Chen, and Y. Zhu, Phys. Rev. B **69**, 085118 (2004).
[11]W. Zhang, Z. Liu, and Z. Wang, Phys. Rev. B **71**, 195114 (2005).
[12]C. Huang and Y. Zhu, AIP Adv. **2**, 042117 (2012).
[13]D. Yudistira, S. Benchabane, D. Janner, and V. Pruneri, Appl. Phys. Lett. **95**, 052901 (2009).
[14]D. Yudistira, S. Benchabane, D. Janner, and V. Pruneri, Appl. Phys. Lett. **98**, 233504 (2011).
[15]D. Morgan, *Surface Acoustic Wave Filters: With Applications to Electronic Communications and Signal Processing*, 2nd ed. (Academic Press, 2007).
[16]D. Yudistira, D. Janner, S. Benchabane, and V. Pruneri, Opt. Express **18**, 27181 (2010).
[17]D. Yudistira, D. Janner, S. Benchabane, and V. Pruneri, Opt. Lett. **34**, 3205 (2009).
[18]M. Yamada, N. Nada, M. Saitoh, and K. Watanabe, Appl. Phys. Lett. **62**, 435 (1993).
[19]B. A. Auld, *Acoustic Fields and Waves in Solids*, 2nd ed. (Krieger Pub Co, 1990).
[20]P. Vairac and B. Cretin, Surf. Interface Anal. **27**, 588 (1999).
[21]R. Rimeika, D. Ciplys, P. Kazdailis, and M. S. Shur, Appl. Phys. Lett. **90**, 181935 (2007).